A Preliminary Analytical and Experimental Investigation of Helicopter Rotor Boundary Layers

DWIGHT A. BLASER* AND HENRY R. VELKOFF†
The Ohio State University, Columbus, Ohio

A momentum-integral technique was developed to calculate the laminar boundary layer on rotating airfoils. This technique was applied to a flat plate and an NACA 0012 airfoil at zero lift under steady rotation. Chordwise and spanwise velocity profiles, wall shear stresses, and separation lines are presented and are found to compare favorably with previous calculations using a finite-difference technique. Experimental velocity data were obtained on a hover stand using dual sensor hot wire probes. Chordwise and spanwise boundary-layer profiles are presented for an NACA 0012 airfoil at zero lift. Similar profiles were observed at various rotor speeds by scaling the y-coordinate. The experimental profiles were found to be "fuller" than those predicted by momentum-integral calculations.

Nomenclature

c	= the chord of the airfoil; units of length
f_{ij}	= coefficients in Eqs. (27) and (28) (defined in Ref. 9)
F, G, H	= velocity profile functions defined by Eqs. (19–21)
p	= pressure; units of force/length^2
Re	= the Reynolds number based on blade chord and free-stream velocity
u, v, w	= local velocities in the x, y, z system of coordinates; units of length/time
U, V, W	= potential velocities in the x, y, z system of coordinates; units of length/time
x, y, z	= rotating curvilinear surface coordinate system shown in Fig. 1; units of length
X, Y, Z	= rotating Cartesian coordinate system shown in Fig. 1; units of length
α	= the angle between the normals to the blade surface and blade chord line
δ	= boundary-layer thickness; units of length
$\delta_1^* \delta_2^*$	= displacement thicknesses in the u and w profiles, respectively; units of length
Δ	= dimensionless form of boundary-layer thickness, $\Omega\delta^2/\nu$
ε	= wall shear stress parameter
η	= dimensionless height above blade surface, y/δ
Θ_{11}, Θ_{12} Θ_{21}, Θ_{22}	= momentum thicknesses of the u and w profiles; units of length (Ref. 9)
$\Lambda_1, \beta_1, \Lambda_2, \beta_2$	= velocity profile parameters defined by Eqs. (22–25)
ν	= kinematic viscosity; units of length^2/time
ρ	= density; units of mass/length^3
τ_B	= two-dimensional, nonrotating surface shear stress; units of force/length^2
τ_{01}, τ_{02}	= components of wall shear stress along chordwise and spanwise directions, respectively; units of force/length^2
$\tau_{or}, \tau_{o\theta}$	= components of wall shear stress along radial and tangential directions, respectively; units of force/length^2
Ω	= rotor speed; units of time^{-1}

Received December 27, 1971; presented as Paper 72-38 at the AIAA 10th Aerospace Meeting, San Diego, Calif., January 17–19, 1973; revision received July 16, 1973. This work was sponsored by the U.S. Army Air Mobility Research and Development Laboratory, Eustis Directorate.

Index categories: Rotary Wing Aerodynamics; Boundary Layers and Convective Heat Transfer—Laminar; Subsonic and Transonic Flow.

* Research Associate, Department of Mechanical Engineering; now Associate Senior Research Engineer at General Motors Research Laboratories, Warren, Mich.

† Professor, Department of Mechanical Engineering; presently, Staff Scientist, U.S. Army Air Mobility R & D Laboratory, Ames Research Center, Moffett Field, Calif.

Introduction

THE design of rotor blades has relied heavily upon the use of two-dimensional airfoil data. By assuming that individual blade elements produce lift independently, a so-called "blade element theory" was developed in the early stages of rotor design. With this theory, it was possible to make estimates of rotor thrust and power requirements without requiring a thorough knowledge of the boundary-layer mechanisms which affect the production of lift and drag. Actual rotors have been observed to perform better than would be expected from "blade element theory" employing steady-state two-dimensional blade section characteristics.[1,2]

Recently, considerable effort has been spent investigating the boundary layers of rotating airfoils in an attempt to explain this improved performance.[3–6] Almost all of this effort has been analytical in nature due to the complexity and expense involved in an experimental program in such a dynamic environment. One of the most recent and notable analytical contributions was made by Dwyer and McCroskey.[6] They utilized a combination finite-difference and relaxation technique to solve the boundary-layer equations governing laminar flow near the surface of a rotating airfoil.

The present investigation consists of an analytical phase and an experimental phase directed towards determining the basic nature of the boundary layer on a helicopter rotor in hover. The analytical phase utilizes momentum-integral methods and thus serves as an indication of the utility and accuracy of this approximate technique. The experimental phase employs hot wire anemometry to obtain boundary-layer measurements on a hovering model rotor blade.

Theoretical Analysis

General Formulation

The present analysis is restricted to blades which are rotated about an axis normal to the axis of the blade. The blade is assumed infinitely long so that there are no end effects. The coordinate system is shown in Fig. 1. The blade chord lies in the X-Z plane with the Z-axis located at the blade leading edge. The Y-axis is the axis of rotation and is located at the leading edge of the blade. The axes are fixed with respect to the blade so that they rotate with constant angular speed Ω. Note that they form a left-hand coordinate system so that the standard two-dimensional terminology, u and v for the primary flow and w for the cross-flow, may be retained. For boundary-layer calculations, it is necessary to define the curvilinear surface

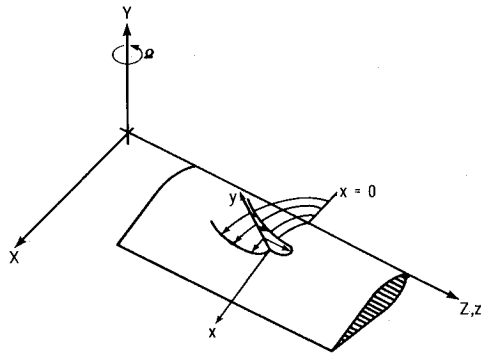

Fig. 1 Rotating coordinate systems.

coordinate system (x, y, z). These coordinates are related to the Cartesian coordinates according to following transformation equations,

$$X = \int_0^x \cos\alpha\, dx - y\sin\alpha \tag{1}$$

$$Y = \int_0^x \sin\alpha\, dx + y\cos\alpha \tag{2}$$

$$Z = z \tag{3}$$

For clarity, x is the chordal distance measured along the surface of the blade from the leading edge, y is the distance above the blade surface measured along a perpendicular to that surface, and z is the blade span measured along the leading edge of the blade.

Momentum-Integral Equations

In order to obtain the momentum-integral equations, we must first begin with the appropriate steady boundary-layer equations in the curvilinear boundary-layer coordinates (x, y, z). These equations are given below for small surface curvature [7]

$$u_x + v_y + w_z = 0 \tag{4}$$

$$uu_x + vu_y + wu_z - 2\Omega w\cos\alpha - \Omega^2 x\cos\alpha = -p_x/\rho + \nu u_{yy} \tag{5}$$

$$uw_x + vw_y + ww_z + 2\Omega u\cos\alpha - \Omega^2 z = -p_z/\rho + \nu w_{yy} \tag{6}$$

Equation (4) is the familiar continuity equation while Eqs. (5) and (6) are the boundary-layer momentum equations along the chordwise and spanwise directions, respectively. In these latter equations, we may identify from left to right the convection, Coriolis, centrifugal, pressure, and viscous terms. The pressure gradients are related to the potential flow velocities by the following relations:

$$\begin{aligned} -p_x/\rho &= UU_x + WU_z - 2\Omega W\cos\alpha - \Omega^2 x\cos\alpha \\ &= UU_x + WW_x - \Omega^2 x\cos\alpha \end{aligned} \tag{7}$$

$$\begin{aligned} -p_z/\rho &= UW_x + WW_z + 2\Omega U\cos\alpha - \Omega^2 z \\ &= UU_z + WW_z - \Omega^2 z \end{aligned} \tag{8}$$

By using the continuity equation to eliminate v and substituting Eqs. (7) and (8), Eqs. (5) and (6) are integrated across the boundary layer. By making the standard definitions for displacement and momentum thicknesses and wall shear stresses (see Ref. 9), the momentum equations assume the following form:

$$\frac{\partial}{\partial x}(U^2\Theta_{11}) + \frac{\partial}{\partial z}(UW\Theta_{12}) + UU_x\delta_1^* + WW_x\delta_2^* = \tau_{01}/\rho \tag{9}$$

$$\frac{\partial}{\partial x}(UW\Theta_{21}) + \frac{\partial}{\partial z}(W^2\Theta_{22}) + UU_z\,\delta_1^* + WW_z\delta_2^* = \tau_{02}/\rho \tag{10}$$

These equations are designated as the three-dimensional momentum-integral equations which are chosen in this analysis to represent the boundary-layer actions in place of Eqs. (4–6). It is reminded that the solution of these equations will indicate an averaged behavior of the boundary-layer flow.

Velocity Profiles

Pohlhausen[8] was first to introduce a general method of solving the two-dimensional momentum-integral equation. The extension of Pohlhausen's technique to the three-dimensional momentum-integral equations involves assuming profile functions for the velocity components, u and w, which may contain a total of two undetermined parameters. To insure that these approximate velocity profiles closely represent those that actually occur, a number of conditions derived from the differential equations and the boundary conditions are imposed at the surface as well as at the junction with the external flow. Those conditions satisfied in this analysis are as follows:

Conditions at the surface

$$u = 0 \qquad w = 0 \tag{11}$$

$$u_{yy} = (1/\nu)[(1/\rho)p_x - \Omega^2 x\cos\alpha]$$

$$w_{yy} = (1/\nu)[(1/\rho)p_z - \Omega^2 z] \tag{12}$$

Conditions at the junction with the external flow

$$u = U \qquad w = W \tag{13}$$

$$u_y = 0 \qquad w_y = 0 \tag{14}$$

$$u_{yy} = 0 \qquad w_{yy} = 0 \tag{15}$$

These conditions insure that, at least at both edges of the boundary layer, the approximate velocity profiles have the appropriate behavior.

The accuracy of the momentum-integral method is dependent upon the characteristic parameters selected to allow the velocity profiles to assume different shapes. In the present analysis, the boundary-layer thickness δ and a wall shear stress parameter ε were selected to represent the growth of the boundary layer on a rotating airfoil. In the early stages of this investigation, ε was defined as the ratio of spanwise to chordwise wall shear stresses; however, the solution diverged for the rotating flat plate problem. The identical problem was then attacked using rotating polar coordinates where ε was defined as the ratio of radial to tangential wall shear stresses. This solution was convergent and stable. Since Cartesian coordinates are preferred for the rotating airfoil cases, the forms for the chordwise and spanwise velocity profiles were generalized from the polar profiles into the following symmetric forms:

$$u/U = F(\eta) + \Lambda_1 G(\eta) + \beta_1 H(\eta) \tag{16}$$

$$w/W = F(\eta) + \Lambda_2 G(\eta) + \beta_2 H(\eta) \tag{17}$$

where in order to satisfy the previously listed boundary conditions the profile functions may be defined by the polynomials

$$\eta = y/\delta \tag{18}$$

$$F(\eta) = 2\eta - 2\eta^3 + \eta^4 = 1 - (1+\eta)(1-\eta)^3 \tag{19}$$

$$G(\eta) = \tfrac{1}{6}(\eta - 3\eta^2 + 3\eta^3 - \eta^4) = \tfrac{1}{6}\eta(1-\eta)^3 \tag{20}$$

$$H(\eta) = 2(\eta - 6\eta^3 + 8\eta^4 - 3\eta^5) = 2\eta(1+3\eta)(1-\eta)^3 \tag{21}$$

The profile parameters Λ_1, β_1, Λ_2, and β_2 are functions of the boundary-layer parameters δ and ε, and the potential flow according to the following relations:

$$\Lambda_1 = [(UU_x + WW_x)/\Omega U]\,\Omega\delta^2/\nu \tag{22}$$

$$\beta_1 = -(W/U)\varepsilon \tag{23}$$

$$\Lambda_2 = [(UU_z + WW_z)/\Omega W]\,\Omega\delta^2/\nu \tag{24}$$

$$\beta_2 = (U/W)\varepsilon \tag{25}$$

The profile shape parameters Λ_1 and Λ_2 evolve directly from the second boundary conditions at the surface. These conditions are obtained by evaluating the chordwise and spanwise Navier-Stokes equations at $y = 0$, and are analogous to the condition used by Pohlhausen[8] in the development of a general two-dimensional momentum-integral method. The parameters β_1 and β_2 were deduced from the flat plate solution in polar coordinates for which

$$\varepsilon = \tau_{or}/\tau_{o\theta} - \Omega\delta^2/12\nu \tag{26}$$

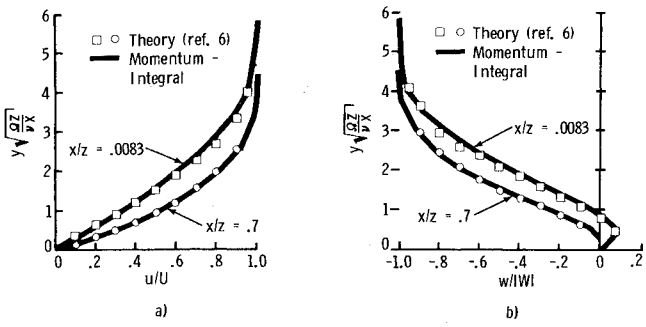

Fig. 2 Comparison of chordwise and spanwise profiles, with Ref. 6 for a flat plate.

Mathematical Equations

The mathematical problem was formulated as follows. The momentum-integral equations have allowed the choice of two free parameters in the velocity profiles. These parameters are δ, the boundary-layer thickness, and ε, a wall shear stress parameter. Throughout the present analysis, $\Delta = \Omega\delta^2/\nu$, a dimensionless form of boundary-layer thickness will be used in place of δ for the first parameter. Using Eqs. (16) and (17), the momentum and displacement thicknesses and the wall shear stresses may be represented as polynomials in the profile parameters Λ_1, β_1, Λ_2, β_2. Furthermore, substitution of these polynomials into Eqs. (9) and (10) results in a pair of equations from which Δ and ε are to be obtained as functions of x and z. After considerable algebraic manipulation, these equations are written in the following form:

$$f_{11}\Delta_x + f_{12}\Delta_z + f_{13}\varepsilon_x + f_{14}\varepsilon_z = f_{15} \quad (27)$$

$$f_{21}\Delta_x + f_{22}\Delta_z + f_{23}\varepsilon_x + f_{24}\varepsilon_z = f_{25} \quad (28)$$

where the functions f_{ij} are complicated functions of x, z, Δ, ε, and the potential flow. These functions are presented in full in Ref. 9.

Equations (27) and (28) were solved using an approximate numerical technique whereby the spanwise derivatives were evaluated numerically, and the resulting differential equations were solved using a step-by-step routine beginning at the blade leading edge. The details of this routine are described in Ref. 9. These calculations were performed on an IBM 360/75 computer, and the results are presented for two airfoils.

Flat Plate, Zero Pressure Gradient

The potential flow for a rotating flat plate is given by $U = \Omega z$ and $W = -\Omega x$. For this simple case, the boundary-layer equations exhibit symmetry with respect to the variable x/z. The momentum-integral equations for this case can be reduced to ordinary differential equations for $\Delta(x/z)$ and $\varepsilon(x/z)$. The results of boundary-layer calculations for a rotating flat plate are presented in Figs. 2 and 3.

The velocity profiles on a rotating flat plate are compared with those of Ref. 6 in Figs. 2a and 2b. The profiles are presented for a position near the leading edge ($x/z = 0.0083$), and a position considerably aft of the leading edge ($x/z = 0.7$). These comparisons indicate that the momentum-integral method could ably replace the finite element calculations for the rotating flat plate. Note that the profiles match those of Ref. 6 with a little better accuracy for $x/z = 0.7$ than for $x/z = 0.0083$. This is reasonable since the flow near the hub is being accelerated due to rotational effects, and the momentum-integral method is known to give better results in two-dimensional accelerated flows.

A second comparison with Dwyer and McCroskey's results for a flat plate is made in Fig. 3. In this figure, the ratio of the chordwise wall shear stress to the equivalent two-dimensional wall shear stress is plotted vs x/z. The two methods agree to within 3% for $x/z \leqq 0.8$. It was shown in Ref. 6 that a fourth-order perturbation analysis was accurate for $x/z \leqq 0.5$; however, beyond this value of x/z, the perturbation solution diverged very rapidly. The momentum-integral technique, representing an averaged boundary-layer behavior, maintains the correct trend through much larger values of x/z.

NACA 0012 Airfoil

Due to the success of the momentum-integral method for the flat plate case, the calculation procedure was applied to a rotating NACA 0012 airfoil at zero lift. This airfoil shape is used for a number of helicopter rotors and was also used throughout the experimental portion of this investigation.

The chordwise potential flow was obtained from the two-dimensional analytical data of Ref. 10. Since derivatives of the potential velocities are also necessary inputs to the calculation procedure, these data were approximated by the following equation:

$$U = \Omega z\{41.0(x/c)e^{-38.4x/c} + [1.245 - 0.267(x/c)](1 - e^{-23.3x/c})\} \quad (29)$$

The spanwise potential flow was obtained from Eq. (29) which was derived from the potential flow solution of Sears.[11]

$$W(x) = W(o) + \int_o^x \left[\frac{U}{Z} - 2\Omega\cos\alpha\right] dx \quad (30)$$

The value of $W(o)$ was evaluated using the approximations developed by Graham.[12]

Chordwise and spanwise velocity profiles are shown in Figs. 4a and 4b for a rotating NACA 0012 airfoil. The results of the momentum-integral analysis are plotted as solid lines for a chordwise position $x/c = 0.6$ and spanwise positions of $z/c = 1$ and $z/c = \infty$. This latter spanwise position corresponds to the two-dimensional chordwise flow profile. The chordwise profiles will be examined first.

The stabilizing effects of rotation are again depicted in the

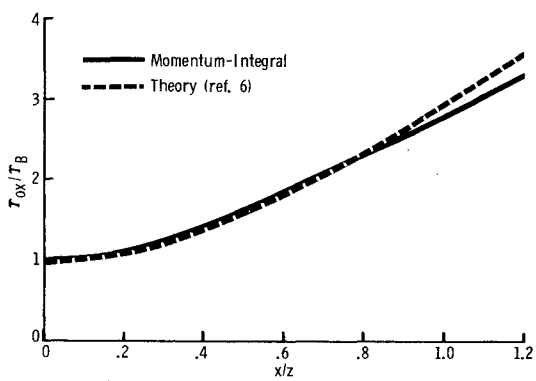

Fig. 3 Chordwise shear stress variation for a rotating flat plate.

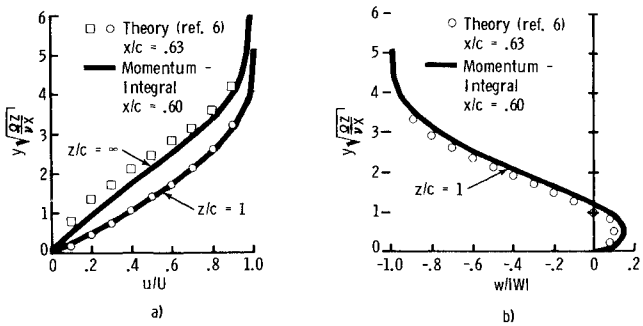

Fig. 4 Comparison of chordwise and spanwise velocity profiles with Ref. 6 for an NACA 0012 airfoil.

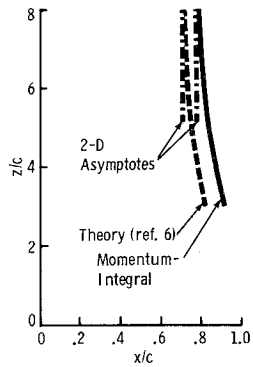

Fig. 5 Comparison of separation lines with Ref. 6 for an NACA 0012 airfoil.

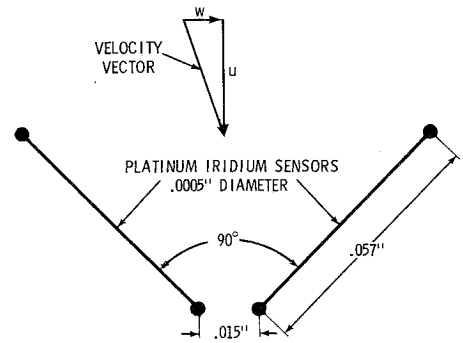

Fig. 7 Physical dimensions of V-configuration hot wire probe.

chordwise profiles of Fig. 4a since the profile at $z/c = 1$ is considerably "fuller" than the equivalent profile at $z/c = \infty$. The results of the finite-difference solution of Ref. 6 are included for comparison. It must be noted that while the results of Ref. 6 are for identical spanwise positions, their chordwise position was at $x/c = 0.63$. The comparison is still quite good, especially for the $z/c = 1$ case.

The spanwise profile at $x/c = 0.6$ and $z/c = 1.0$ is shown in Fig. 4b. The data from Ref. 6 are again included for comparison. The spanwise flow exhibits considerably more outflow than was observed in the profiles on a rotating flat plate. This greater outflow can be attributed to the deceleration in the chordwise potential flow. As the chordwise flow slows down, continuity must still be preserved; therefore, the spanwise flow acts as a flow relief and reduces the rate of boundary layer growth.

The separation line determined from the momentum-integral analysis for the 0012 airfoil is shown in Fig. 5. This figure illustrates the first real discrepancy between the results of Ref. 6 and those presented in this study. That is, the two-dimensional asymptote from the momentum-integral analysis occurs at $x/c = 0.77$ while that reported in Ref. 6 occurs at $x/c = 0.70$. The aft movement of the separation line as z decreases appears to be quite similar for both methods.

Experimental Study

Test Equipment

The rotor test stand used to simulate model rotor hover conditions was powered by two air motors. The model rotor blade had a diameter of 8 ft, a chord length of 9 in., and an NACA 0012 airfoil section. The blade was untwisted.

Constant temperature anemometer amplifier systems were used to obtain the velocity data. Two printed circuit boards used in commercial anemometers were purchased and customized into a dual anemometer amplifier package that was mounted on the rotor hub. In this manner, the data signals were amplified prior to being transmitted via slip rings to the data console. Linearizer units were used which made the hot wire sensitivity nearly uniform over a wide range of velocities.

The hot wire probe is shown attached to the rotor blade in Fig. 6 as viewed from the blade tip. The anemometer amplifier package which is attached to the rotor hub can be seen in the background. The wires are arranged in a V-configuration which permitted them to be placed at the same distance from the blade surface during the tests. The physical dimensions of this arrangement are shown in Fig. 7. The two sensors, placed in this configuration, permit measurements of the velocity vector which was resolved into chordwise and spanwise velocity components.

Test Procedure

The plane of the hot wire sensors was made parallel to the blade surface by the apparatus pictured in Fig. 8. It consists of a traversing microscope and associated mechanism to attach the microscope rigidly to the blade. By viewing the probe and probe surface simultaneously through the 100x lens of the microscope, the probe could be aligned accurately. After the probe was locked in the desired position, the traversing microscope was used to measure the perpendicular distance from the blade surface to the sensor plane. This traversing mechanism permitted a readability to the nearest 0.0001 in. Measurements were made from 0.1 in. to 0.002 in. to cover the complete boundary-layer flow.

The tests were conducted in the following sequence. The chordwise and spanwise positions were chosen and the probe aligned at this surface position by the technique just described. The probe was set at a position near 0.1 in. to represent a condition outside the boundary layer. At this probe position,

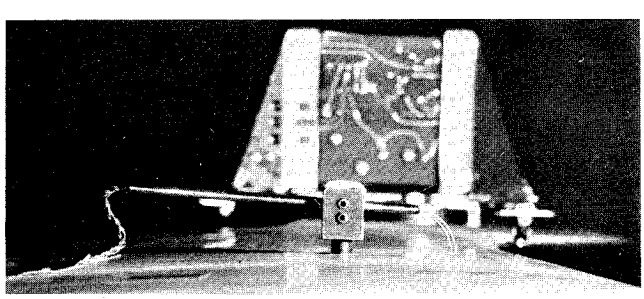

Fig. 6 Hot wire probe mounted on rotor blade as viewed from the blade tip.

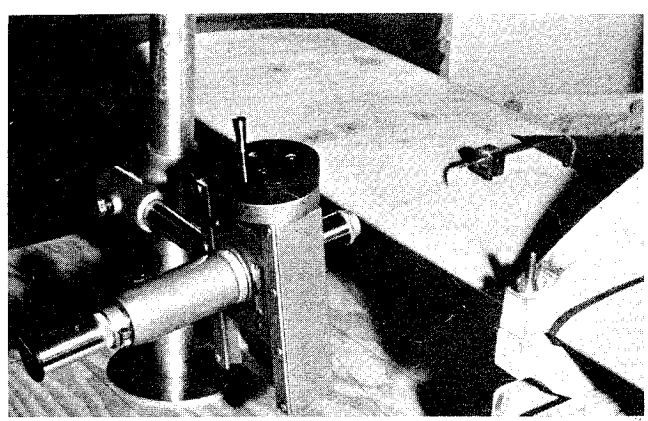

Fig. 8 Traversing microscope attached to rotor blade during probe height measurement.

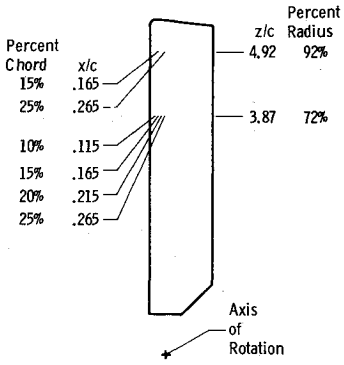

Fig. 9 Location of hot wire data on rotor blade.

tests were conducted at rotor speeds of 100, 200, 300, and 400 rpm. The probe was then lowered and tests repeated until data were obtained across the entire boundary layer. This sequence of tests required the fewest adjustments of the probe and minimized the possibility of accidental probe damage from contact with the sensors. While examining the velocity data one should keep in mind that the rotor had to be stopped, the probe position adjusted, and the hover conditions reproduced between data points.

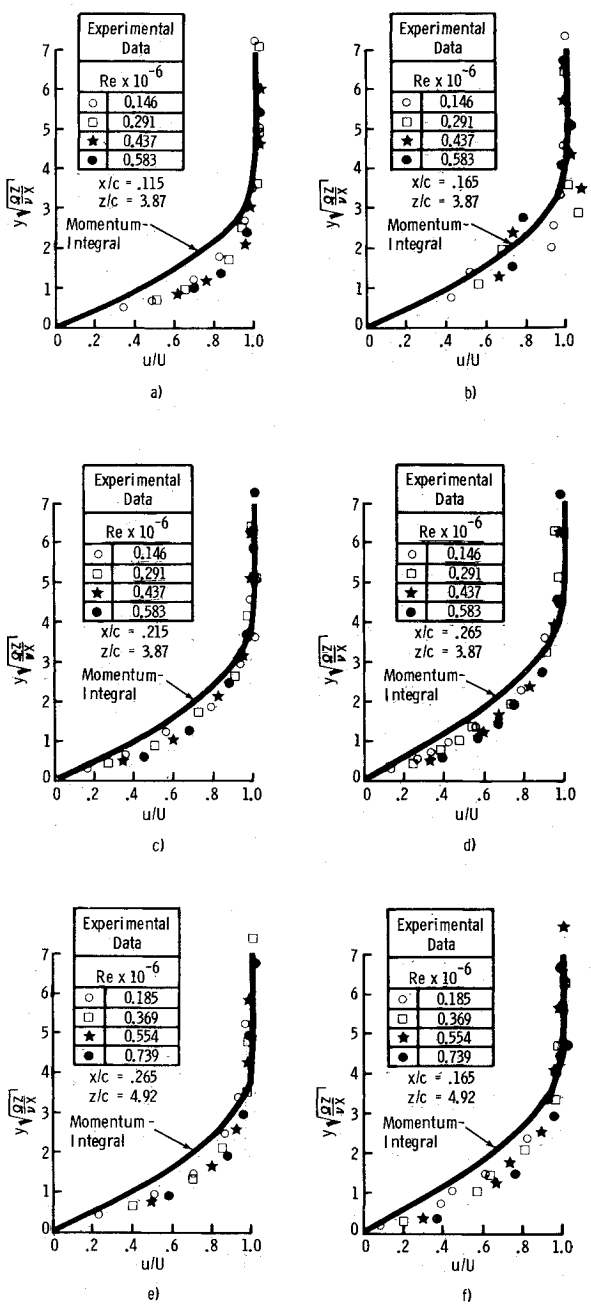

Fig. 10 Chordwise velocity profiles on an NACA 0012 at zero lift.

Results and Discussion

The experimental hot wire data at zero lift were obtained at spanwise locations of $z/c = 3.87$ and $z/c = 4.92$. The chordwise locations at which velocity profiles were obtained are indicated in Fig. 9. The relationships between z/c and percent radius are shown along with the relationships between x/c and percent chord. At $z/c = 3.87$, the Reynolds numbers based on the blade chord are 0.146, 0.291, 0.437 and 0.583 million which correspond to rotor speeds of 100, 200, 300, and 400 rpm, respectively. At these rotor speeds, the Reynolds numbers at $z/c = 4.92$ are 0.185, 0.369, 0.554, and 0.739 million, respectively.

Figs. 10a through 10f present chordwise velocity profiles on a rotating NACA 0012 airfoil at zero lift. By plotting vs the "stretched" boundary layer cordinate, $y(\Omega z/\nu x)^{1/2}$, used in the analytical study, the data at different rotor speeds or Reynolds numbers were combined into a single graph. The solid line in each of these figures indicates the velocity profile predicted by the momentum-integral analysis. At each location on the blade, the experimental data indicate a "fuller" profile than the analytical calculations.

Except for Fig. 10b, the experimental chordwise velocity data congregate quite well for the range of Reynolds numbers presented. The data presented in this figure represent the very first rotor hot wire data obtained in this study. Since the positioning of the probe was accomplished by visually viewing the probe through the microscope, the consistency of the data depended greatly on the technique used while adjusting the probe height. After this first profile was completed, the consistency of the data appears to be much improved.

Spanwise velocity data were also derived from the V-configuration hot wire measurements at the zero lift condition. A typical set of profiles are shown in Fig. 11 using the same scaling of the y-coordinate used earlier for the chordwise profiles. Once again, this scaling tends to congregate the profiles obtained at various Reynolds numbers.

The theoretical spanwise profiles as calculated using the momentum-integral analysis are also shown in Fig. 11. The location of the axis of rotation in these theoretical calculations was found to greatly influence the shape of the spanwise profile. The solid line represents that profile for rotation about an axis located at the leading edge while the dashed line represents similar calculations for the axis located at the quarter chord position. Since the model rotor used in the experimental study was also rotated about an axis located at the quarter chord, this later calculation more accurately follows the data trend. The spanwise experimental profiles are observed to be "fuller"

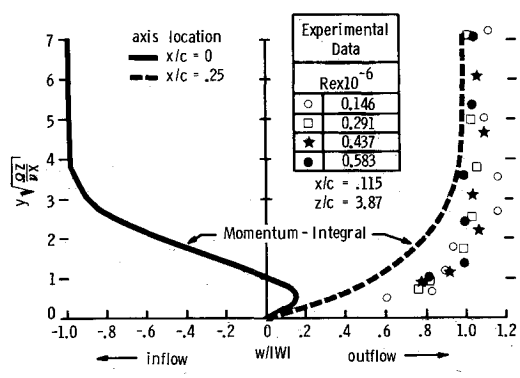

Fig. 11 Spanwise profiles on an NACA 0012 at $x/c = 0.115$ and $z/c = 3.87$ and at zero lift.

than the analytical calculations in a manner similar to that observed in the chordwise profile comparisons of Fig. 10.

It is interesting to note that shifting the axis of rotation from the leading edge to the quarter chord had a negligible effect on the theoretically calculated chordwise velocity profiles presented in Fig. 10.

Conclusions

The momentum-integral method, combined with the numerical solution technique, provided an accurate engineering approach to three-dimensional rotating boundary-layer calculations. The comparisons with the so-called "exact" solutions of Ref. 6 provided sound evidence of the capability of this momentum-integral technique. The location of the axis of rotation was found to greatly influence the shape of the spanwise velocity profiles and to have negligible effect on the chordwise profiles.

The hot-wire anemometer instrumentation provided the most significant results of this study. These data indicate that the chordwise and spanwise velocity profiles are much "fuller" than those calculated using the momentum-integral analysis. It is believed that data provided by this portion of the study will serve as a foundation for future analytical and experimental research.

References

[1] Himmelskamp, H., "Profiluntersuchungen an einem umlaufenden Propeller," *Mitteibungen der Max-Planck Institut*, No. 2, 1950.

[2] Harris, F. D., "Preliminary Study of Radial Flow Effects on Rotor Blades," *Journal of the American Helicopter Society*, Vol. 11, No. 1, 1966.

[3] Banks, W. H. H. and Gadd, G. E., "Delaying Effects of Rotation on Laminar Separation," *AIAA Journal*, Vol. 1, No. 4, April 1963, pp. 941–942.

[4] Velkoff, H. R., "A Preliminary Study of the Effect of a Radial Pressure Gradient on the Boundary Layer of a Rotor Blade," *Proceedings of the CAL/USAAVLABS Symposium on Aerodynamic Problems Associated with V/STOL Aircraft*, Vol. III, Cornell Aeronautical Lab., Buffalo, N.Y., 1966.

[5] McCroskey, W. J. and Yaggy, P. F., "Laminar Boundary Layers on Helicopter Rotors in Forward Flight," *AIAA Journal*, Vol. 6, No. 10, Oct. 1968, pp. 1919–1926.

[6] Dwyer, H. A. and McCroskey, W. J., "Crossflow and Unsteady Boundary-Layer Effects on Rotating Blades," AIAA Paper 70–50, New York, 1970.

[7] Fogarty, L. E., "The Laminar Boundary Layer on a Rotating Blade," *Journal of the Aeronautical Science*, Vol. 18, No. 4, 1951, pp. 247–252.

[8] Pohlhausen, K., "Zur naherungsweisen Integration der Differentialgleichungen der laminaren Grenzschicht," *Zeitschrift für Angewandte Mathematik und Mechanik*, Vol. I, 1921, pp. 252–268.

[9] Velkoff, H. R., Blaser, D. A., and Hoffman, J. D., "Investigation of Boundary Layers and Tip Flows of Helicopter Rotor Blades," TR 71-73, May 1972, U.S. Army Air Mobility Research and Development Lab., Fort Eustis, Va.

[10] Abbott, I. H. and von Doenhoff, A. E., *Theory of Wing Sections*, Dover, New York, 1959.

[11] Sears, W. R., "Potential Flow Around a Rotating Cylindrical Blade," *Journal of the Aeronautical Science*, Vol. 17, 1950, p. 183.

[12] Graham, M. E., "Calculation of Laminar Boundary Layer Flow on Rotating Blades," Ph.D. thesis, 1950, Cornell Univ., Ithaca, N.Y.